

This is a repository copy of *Dealing with contaminants in Coulomb excitation of radioactive beams*.

White Rose Research Online URL for this paper:

<https://eprints.whiterose.ac.uk/172836/>

Version: Published Version

---

**Article:**

Morrison, L., Hadyńska-Klęk, K., Podolyák, Zs et al. (35 more authors) (2020) Dealing with contaminants in Coulomb excitation of radioactive beams. Journal of Physics: Conference Series. 012146. ISSN 1742-6596

<https://doi.org/10.1088/1742-6596/1643/1/012146>

---

**Reuse**

This article is distributed under the terms of the Creative Commons Attribution (CC BY) licence. This licence allows you to distribute, remix, tweak, and build upon the work, even commercially, as long as you credit the authors for the original work. More information and the full terms of the licence here:

<https://creativecommons.org/licenses/>

**Takedown**

If you consider content in White Rose Research Online to be in breach of UK law, please notify us by emailing [eprints@whiterose.ac.uk](mailto:eprints@whiterose.ac.uk) including the URL of the record and the reason for the withdrawal request.

PAPER • OPEN ACCESS

## Dealing with contaminants in Coulomb excitation of radioactive beams

To cite this article: L Morrison *et al* 2020 *J. Phys.: Conf. Ser.* **1643** 012146

View the [article online](#) for updates and enhancements.



The Electrochemical Society  
Advancing solid state & electrochemical science & technology

**240th ECS Meeting** ORLANDO, FL

Orange County Convention Center Oct 10-14, 2021



Abstract submission due: April 9

**SUBMIT NOW**

# Dealing with contaminants in Coulomb excitation of radioactive beams

L Morrison<sup>1</sup>, K Hadyńska-Klęk<sup>2,1</sup>, Zs Podolyák<sup>1</sup>, L P Gaffney<sup>4,8</sup>, L Kaya<sup>5</sup>, T Berry<sup>1</sup>, A Boukhari<sup>6</sup>, M Brunet<sup>1</sup>, R Canavan<sup>1,7</sup>, R Catherall<sup>8</sup>, S J Colosimo<sup>4</sup>, J G Cubiss<sup>9</sup>, H De Witte<sup>10</sup>, D T Doherty<sup>1</sup>, Ch Fransen<sup>5</sup>, E Giannopoulos<sup>8,11</sup>, H Grawe<sup>3</sup>, H Hess<sup>5</sup>, T Kröll<sup>3</sup>, N Lalović<sup>12</sup>, B Marsh<sup>8</sup>, Y Martinez Palenzuela<sup>8,10</sup>, G O'Neill<sup>13,14</sup>, J Pakarinen<sup>11</sup>, J P Ramos<sup>8</sup>, P Reiter<sup>5</sup>, J A Rodriguez<sup>8</sup>, D Rosiak<sup>5</sup>, S Rothe<sup>8</sup>, M Rudigier<sup>1</sup>, M Siciliano<sup>15,16</sup>, E C Simpson<sup>17</sup>, P Spagnoletti<sup>13</sup>, S Thiel<sup>5</sup>, N Warr<sup>5</sup>, F Wenander<sup>8</sup>, R Zidarova<sup>8</sup> and M Zielińska<sup>15</sup>

<sup>1</sup> Department of Physics, University of Surrey, Guildford, GU2 7XH, United Kingdom

<sup>2</sup> Heavy Ion Laboratory, University of Warsaw, Ludwika Pasteura 5A, 05-077 Warszawa, Poland

<sup>3</sup> GSI Helmholtzzentrum für Schwerionenforschung, Planckstrasse 1, 64291 Darmstadt, Germany

<sup>4</sup> Oliver Lodge Laboratory, University of Liverpool, Liverpool, L69 7ZE, United Kingdom

<sup>5</sup> IKP Köln, Zülpicher Str. 77, 50937 Köln, Germany

<sup>6</sup> Université de Paris-Sud 11, 15 Rue Georges Clemenceau, 91400 Orsay, France

<sup>7</sup> National Physical Laboratory, Hampton Rd, Teddington, TW11 0LW, United Kingdom

<sup>8</sup> CERN, Physics Department, 1211 Geneva 23, Switzerland

<sup>9</sup> University of York, Heslington, York, YO10 5DD, United Kingdom

<sup>10</sup> KU Leuven, Instituut voor Kern-en Stralingsfysica, B-3001 Leuven, Belgium

<sup>11</sup> Department of Physics, University of Jyväskylä, P.O. Box 35 (YFL), Jyväskylä, FI-40014, Finland

<sup>12</sup> Physics Department, Lund University, Box 118, Lund SE-221 00, Sweden

<sup>13</sup> School of Computing, Engineering and Physical Sciences, University of the West of Scotland, Paisley PA1 2BE, UK

<sup>14</sup> iThemba LABS, Old Faure Road, Faure, Cape Town, 7131, South Africa

<sup>15</sup> IRFU, CEA, Université Paris-Saclay, F-91191 Gif-sur-Yvette, France

<sup>16</sup> INFN Laboratori Nazionali di Legnaro, 35020 Legnaro (Pd), Italy

<sup>17</sup> Department of Nuclear Physics, Research School of Physics, Australian National University, Canberra ACT 2601, Australia

E-mail: [l.morrison@surrey.ac.uk](mailto:l.morrison@surrey.ac.uk)

## Abstract.

Data analysis of the Coulomb excitation experiment of the exotic  $^{206}\text{Hg}$  nucleus, recently performed at CERN's HIE-ISOLDE facility, needs to account for the contribution to target excitation due to the strongly-present beam contaminant  $^{130}\text{Xe}$ . In this paper, the contamination subtraction procedure is presented.



## 1. Introduction

One commonly used method to study the electromagnetic structure of the atomic nucleus is the technique of Coulomb excitation. The experiment to study low-lying collective structure of two proton-hole  $^{206}\text{Hg}$  located near the heaviest doubly-magic nucleus  $^{208}\text{Pb}$  was performed in November 2017 at CERN-ISOLDE. Here,  $^{208}\text{Pb}$  acts as a shell model ‘core’ from which nuclear excitations in  $^{206}\text{Hg}$  occur, therefore the intrinsic nuclear properties of  $^{206}\text{Hg}$  provide a good probe of shell model validity in this region of the Segré chart.

A radioactive  $^{206}\text{Hg}$  beam was post-accelerated to 4.195 MeV/u energy with  $\sim 7.75 \times 10^5$  pps intensity and delivered to a  $^{94}\text{Mo}$  target. The scattered particles were detected using a double-sided silicon strip detector (DSSSD) placed downstream, allowing an annular coverage of between 20 and 59°. Coincident  $\gamma$ -ray events were used to observe de-excitation of Coulomb-excited states in either the projectile or recoiling target-like nuclei using 23 HPGe detectors comprising the MINIBALL array [1].

$^{94}\text{Mo}$  is a stable isotope and the electromagnetic properties of this nucleus in the low-spin region are well-known, hence the observed excitation of the  $^{94}\text{Mo}$  target can serve as normalisation in the analysis of the  $^{206}\text{Hg}$  data performed using the GOSIA code [2, 3]. To apply the normalisation procedure, the amount of target excitation due exclusively to the interaction with  $^{206}\text{Hg}$  must be precisely known. When beam contamination is present, its contribution to the observed target excitation must be carefully subtracted.

A number of intense peaks arising from Coulomb excitation of  $^{130}\text{Xe}$  were observed in the data from the recent experiment focused on  $^{206}\text{Hg}$ . The presence of this xenon isotope in the  $\gamma$ -ray spectrum had to be accounted for in order to progress with the  $^{206}\text{Hg}$  data analysis, and as such became an initial focus of the current project. A procedure of isobaric contamination subtraction is outlined in Ref. [4], however in the event of the presence of contaminants with a different mass than the beam of interest, a different analysis approach is required. In this paper a new such method of the contamination subtraction is presented.

## 2. Presence of $^{130}\text{Xe}$ in the data

The appearance of xenon in the collected data is not unexpected due firstly to its natural presence in the atmosphere arising from cometary and chondritic origins [5], but also as a result of the purification procedure for the buffer gas in the REXTRAP not completely eliminating other noble gases during chemical separation.  $^{130}\text{Xe}$  has a natural abundance of only 4.07%, but the reason this isotope was present and strongly Coulomb-excited during this experiment was due to a number of parallel contributory factors.

The charge state for  $^{206}\text{Hg}$  of  $46^+$  ( $A/Q = 4.478$ ) was chosen so as to maximise REX-EBIS efficiency, and the time structure of the beam. The  $^{130}\text{Xe}$  isotope with charge state  $29^+$  has the mass over charge ratio ( $A/Q = 4.483$ ) very close to that of  $^{206}\text{Hg}$ . It happens to be the case that this particular charge state of  $^{130}\text{Xe}$  was not totally cleaned from within the REX separator, and therefore was delivered to MINIBALL as a contaminant species.

In addition, a higher degree of collectivity and probability of excitation in  $^{130}\text{Xe}$  exists compared to  $^{206}\text{Hg}$ . Due to the proximity to doubly-magic  $^{208}\text{Pb}$ , the first excited state in  $^{206}\text{Hg}$  is at an energy of 1068 keV, and the  $B(E2; 2_1^+ \rightarrow 0_1^+)$  value is predicted to be  $\approx 4$  W.u., while the first  $2_1^+$  state in  $^{130}\text{Xe}$  is placed at 536 keV and decays to the ground state with a  $B(E2; 2_1^+ \rightarrow 0_1^+)$  value of 38(5) W.u. [6]. This translates into a much larger Coulomb-excitation cross section to populate the excited states in  $^{130}\text{Xe}$  compared to that for  $^{206}\text{Hg}$ .

## 3. The role of contaminant subtraction

The two-body reaction kinematics of both  $^{206}\text{Hg} + ^{94}\text{Mo}$  and  $^{130}\text{Xe} + ^{94}\text{Mo}$  systems were simulated using the code available at: <https://github.com/lpgaff/kinsim/blob/master/kinsim3.cc> in order to visualise what the particle spectra for both combinations should look like. The energy

loss in the target material was calculated using the SRIM code [7] and taken into account in the simulations. The results are presented in Figure 1. In both top panels, the target recoil behaviour is similar, however the projectile kinematics are very different. In order to determine the particle gate position, the two plots can be overlaid, as presented in the bottom panel of Figure 1. It is apparent that the beam and target kinematics lines overlap in both cases.

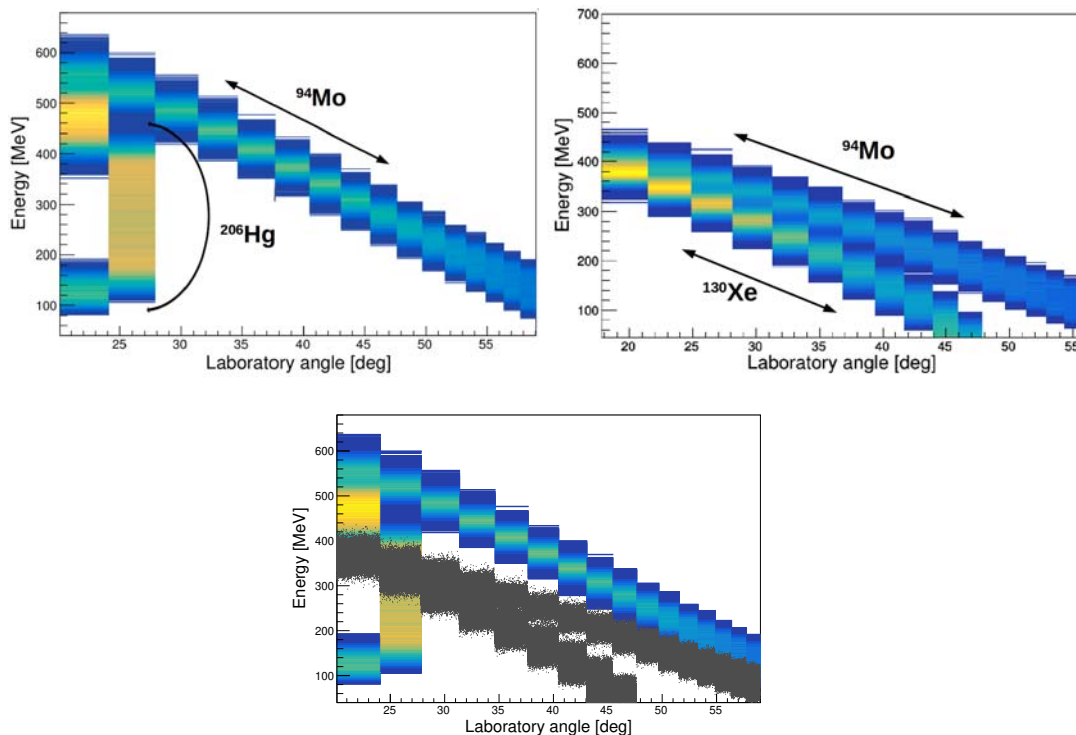


**Figure 1.** Simulated kinematics plots. Panel top left:  $^{206}\text{Hg}+^{94}\text{Mo}$  reaction. Panel top right:  $^{130}\text{Xe}+^{94}\text{Mo}$  reaction. Bottom panel:  $^{206}\text{Hg}+^{94}\text{Mo}$  and  $^{130}\text{Xe}+^{94}\text{Mo}$  kinematic plots overlaid. In both top panels the target recoil kinematics are displayed as the uppermost diagonal line on the plot. In bottom panel the  $^{206}\text{Hg}$  beam on  $^{94}\text{Mo}$  target is given using the contoured lines, and the  $^{130}\text{Xe}$  beam on  $^{94}\text{Mo}$  as the grey points. The  $x$ -axis range for all figures is chosen so as to replicate the DSSSD detector coverage.

When the beam impinges on the target, both reaction partners are excited by one another via an electromagnetic interaction. This means that the beam and target could be Coulomb-excited not only by those isotopes of interest, but also by contaminants within the reaction partner. From Figure 1, it is instantly clear that these cannot be completely separated, and that the excitation of the target  $^{94}\text{Mo}$  originates not only from the interaction with  $^{206}\text{Hg}$ , but also with  $^{130}\text{Xe}$ .

During the  $^{206}\text{Hg}$  Coulomb excitation data analysis, normalisation to known spectroscopic information in the  $^{94}\text{Mo}$  target was applied following the procedure described in Ref. [4]. This technique requires the measured intensities of gamma-ray transitions in Coulomb-excited target nuclei as an input to the GOSIA code analysis. In the present experiment, the transition intensities measured for  $^{94}\text{Mo}$  are skewed if additional excitation occurs as a result of the strong presence of the  $^{130}\text{Xe}$  contaminant. The number of counts as a result of target excitation by a contaminant must be carefully determined and subtracted from the measured intensities of transitions in  $^{94}\text{Mo}$  that are used in the final analysis of the  $^{206}\text{Hg}$  isotope.

## 4. Data cleanup procedure

### 4.1. Kinematics gates

In the Coulomb excitation experiment of  $^{206}\text{Hg}$ , alternate runs were taken with the  $^{206}\text{Hg}$  beam ‘turned off’ (beam gate from the primary target closed), allowing more detailed examination of possible contaminants from the REX-EBIS charge breeder. In the period when  $^{206}\text{Hg}$  was not delivered, excitation of the  $^{94}\text{Mo}$  target was induced exclusively by the  $^{130}\text{Xe}$  contaminant.

The first stage in subtracting the contribution of  $^{130}\text{Xe}$  from the  $(^{206}\text{Hg}+^{130}\text{Xe})+^{94}\text{Mo}$  measured  $\gamma$ -ray spectrum was done by applying kinematic gates around the beam and target in the particle spectra from both the  $^{130}\text{Xe}+^{94}\text{Mo}$  and  $(^{206}\text{Hg}+^{130}\text{Xe})+^{94}\text{Mo}$  data collected in the DSSSD detector. An experimental CD spectrum is presented in Figure 2 with the gates for  $^{206}\text{Hg}$  applied and shown overlaid.

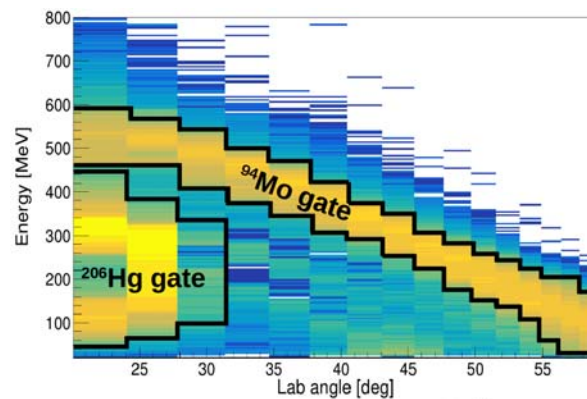


**Figure 2.** Experimental particle spectrum produced after applying the gates drawn using the black lines around the  $^{206}\text{Hg}$  beam and  $^{94}\text{Mo}$  target.

The effect of particle gating presented in Figure 2 on the collected  $\gamma$ -ray spectrum is shown in Figure 3 where the target-particle gated spectrum, Doppler corrected for  $^{206}\text{Hg}$ , is presented. It is evident that this procedure allows unwanted events from the spectrum to be removed. Although the target-particle gated  $\gamma$ -ray spectrum is significantly improved, the remaining prominent structure between 500 and 600 keV, corresponding to the  $2_1^+ \rightarrow 0_1^+$  transition in  $^{130}\text{Xe}$ , indicates that the contaminant is not completely cleaned by the gating procedure and a subtraction is still required.

### 4.2. Subtraction of the contamination $\gamma$ -ray spectrum

The final step in removing the contaminant was to subtract the  $\gamma$ -ray spectrum collected with the  $^{130}\text{Xe}$  beam only from the one measured in  $(^{206}\text{Hg}+^{130}\text{Xe})+^{94}\text{Mo}$  runs. Firstly, data taken with the  $^{206}\text{Hg}$  beam turned off (i.e. solely with the contaminant) was sorted separately, and the same kinematic gates, as well as the Doppler correction according to the velocity of  $^{206}\text{Hg}$  were applied. The obtained  $\gamma$ -ray spectrum is presented in the left panel of Figure 4, and clearly shows the prominent Doppler-broadened peaks arising from transitions in  $^{130}\text{Xe}$ .

This spectrum was then subtracted from that collected in  $(^{206}\text{Hg}+^{130}\text{Xe})+^{94}\text{Mo}$  measurements using a user-defined factor, determined by taking the ratio of intensities in the  $2_1^+ \rightarrow 0_1^+$  peak of  $^{130}\text{Xe}$ . The right panel in Figure 4 displays both the unsubtracted and subtracted  $\gamma$ -ray spectra for  $^{206}\text{Hg}$ . Most noticeably, the 536 keV peak arising from the  $2_1^+ \rightarrow 0_1^+$  transition in  $^{130}\text{Xe}$  has been eliminated. Due to the application of a like-for-like subtraction technique by using exactly the same gates in the  $^{130}\text{Xe}$ -only data set as those used in the  $^{206}\text{Hg}+^{130}\text{Xe}$  data, an appropriate reduction in number of counts in the  $^{94}\text{Mo}$  peak was applied.

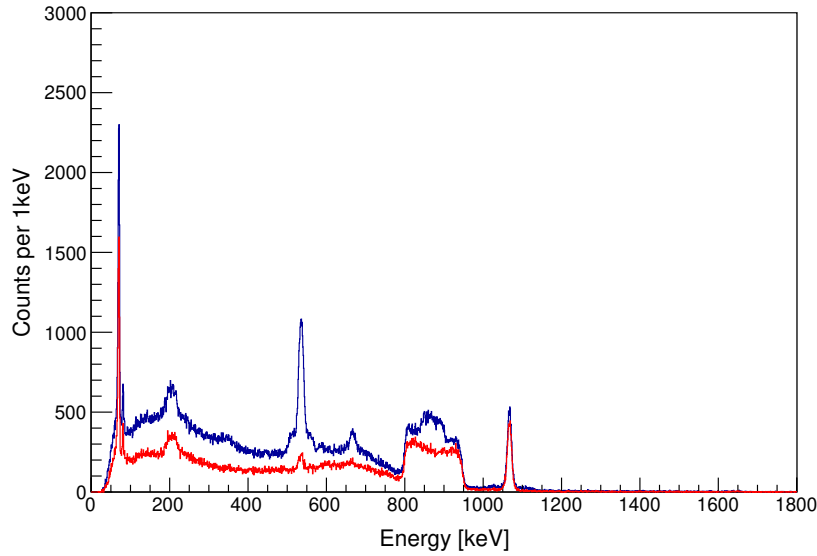


**Figure 3.**  $\gamma$ -ray spectrum for  $^{206}\text{Hg}$  prior to (blue), and post (red) application of appropriate kinematic gates.

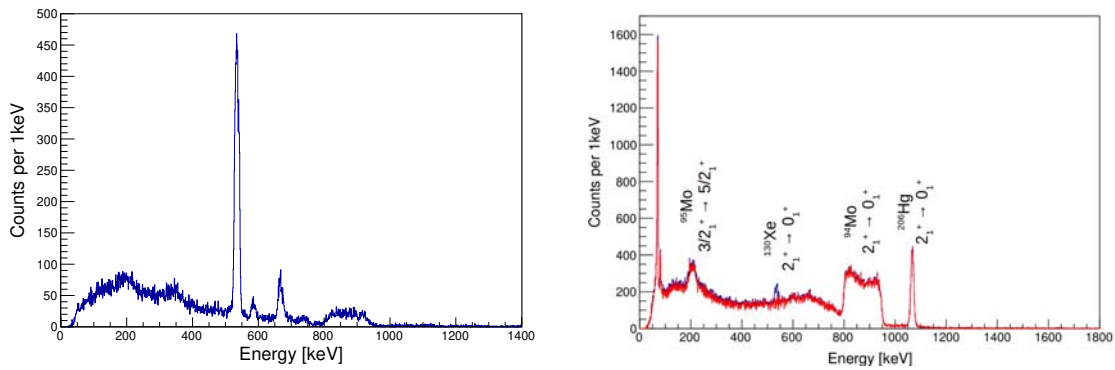


**Figure 4.**  $\gamma$ -ray spectrum post-application of kinematic gates for (left panel):  $^{130}\text{Xe}$  on  $^{94}\text{Mo}$  only, and (right panel):  $^{206}\text{Hg}$  on a  $^{94}\text{Mo}$  target, Doppler corrected for  $^{206}\text{Hg}$ , showing the unsubtracted (with  $^{130}\text{Xe}$ ) data in blue and subtracted (without  $^{130}\text{Xe}$ ) data in red.

## 5. Conclusion

The determination of and correction for the contribution of target excitation due to  $^{130}\text{Xe}$  in the  $^{206}\text{Hg}$  Coulomb excitation experiment was developed and successfully applied.

Cross-checking with simulations verified the validity of kinematic gates, and a multi-step subtraction method was effective as not only did the peaks arising from the excited  $^{130}\text{Xe}$  contamination disappear, but also the number of counts in the transitions in  $^{94}\text{Mo}$  were reduced accordingly, and thus the target excitation effect by  $^{130}\text{Xe}$  was accounted for without further corrections of the measured  $\gamma$ -ray intensities.

## 6. Acknowledgments

The research leading to these results has received funding from the European Union's Horizon 2020 research and innovation programme under grant agreement no. 654002 + 665779 CERN (COFUND). Support from Science and Technology Facilities Council through grants ST/P005314/1, ST/L005743/1, ST/R004056/1, and ST/J000051/1 (UK), and German BMBF under contract 05P18PKCIA + "Verbundprojekt" 05P2018 are acknowledged.

## References

- [1] Warr N, Van de Walle J *et al.* 2013 The Miniball spectrometer *Eur. Phys. J. A* **49**: 40
- [2] Czosnyka T, Cline D and Wu C Y 1982 GOSIA Coulomb excitation data analysis code *Bull. Am. Phys. Soc.* **28**, 745 <http://slcj.uw.edu.pl/en/gosia-code/>
- [3] Cline D Nuclear shapes studied by Coulomb excitation 1986 *Annu. Rev. Nucl. Part. Sci.* **36**, 683
- [4] Zielińska M, Gaffney L P, K. Wrzosek-Lipska K, Clément E, Grahn T, Kesteloot N, Napiorkowski P, Pakarinen J, Van Duppen P, and Warr N 2016 Analysis methods of safe Coulomb-excitation experiments with radioactive ion beams using the GOSIA code *Eur. Phys. J. A* **52** 99
- [5] Avise G, Marty B, Burgess R, Hofmann A, Philippot P, Zahnle K and Zakharov D 2018 Evolution of atmospheric xenon and other noble gases inferred from Archean to Paleoproterozoic rocks *Geochim. Cosmochim. Acta* **232** 82-100
- [6] Singh B 2001 Nuclear Data Sheets for A = 130 *Nucl. Data Sheets* **93**, 33
- [7] Ziegler J F 2013 SRIM The Stopping and Range of Ions in Matter <http://www.srim.org/SRIM/SRIMLEGL.htm>